Revision 1

Temperature-induced amorphization of Na-zeolite A: A view from multi-nuclear high-resolution solid-state NMR

Kim, Hyun Na[1,] and Lee, Sung Keun[1,*]

School of Earth and Environmental Sciences

Seoul National University

Seoul, 151-742 Korea

*Corresponding author,

Lee, Sung Keun

School of Earth and Environmental Sciences,

Seoul National University, Seoul, 151-742, Republic of Korea

E-mail: sungklee@snu.ac.kr

Web: http://plaza.snu.ac.kr/~sungklee

Phone: 82-2-880-6729

Fax: 82-2-871-3269

Revised version submitted to "American Mineralogist" (MS#4928)

5-2-2014

ABSTRACT

Despite efforts to understand the amorphization mechanisms of zeolites upon heating and subsequent dehydration, little is known about the extent of Si-Al disorder and topological variations in both crystalline and amorphous phases during amorphization. In this study, we investigated the atomic structure and the extent of configurational disorder (e.g., Si-Al ordering) in Na-zeolite A and other dehydrated phases during their temperature-induced amorphization using multi-nuclear solid-state NMR. We also report the first multi-nuclear (^{17}O, ^{29}Si, and ^{27}Al) NMR spectra of the intermediate amorphous phases. ^{29}Si MAS NMR results confirm the prevalence of amorphous phases up to ~ 1073 K and variation in Q-species for the crystalline phases. The ^{27}Al quadrupolar coupling constant of the $^{[4]}$Al peak in Na-zeolite A and the intermediate amorphous phases increase with increasing temperature, which suggests an increase in the topological disorder associated with the structural distortion around $^{[4]}$Al. 2D ^{17}O 3QMAS NMR spectra resolve the crystallographically distinct Si-O-Al sites in Na-zeolite A and three types of oxygen linkages namely, Si-O-Al, Si-O-Si, and Al-O-Al in the intermediate amorphous phases, which provides an unambiguous experimental evidence for an increase in the Si-Al disorder during the amorphization of zeolite. The detailed structural changes in Na-zeolite A and other dehydrated phases at various temperatures provide insights into the structural changes of other aluminosilicates during amorphization, thereby highlighting the changes in Si-Al ordering.

INTRODUCTION

Zeolites are a group of microporous aluminosilicate minerals, which are commonly found in diverse geologic environments such as lake, land surfaces, deep-sea sediments, pyroclastic volcanic deposits associated with burial diagenesis, and hydrothermal alteration (Hay and Sheppard, 2001, and see references therein). Zeolites have a range of industrial applications as catalysts, adsorbents, and ion exchangers (Boyd et al., 1947; Breck et al., 1956; Coronas and Santamaria, 2004; Greaves et al., 2005; Greaves et al., 2003a; Kokotailo and Fyfe, 1989;

Mintova and Bein, 2001). The three-dimensional networks of zeolites consist of corner-sharing AlO_4 and SiO_4 tetrahedrons and charge balancing cations such as Na and Ca. The zeolite network is known to collapse and transform into an amorphous phase upon heating. The temperature-induced amorphization of zeolites with the accompanying structural changes has long been investigated in many experimental and theoretical studies owing to the fundamental and technological interests (Bursill and Thomas, 1981; Colyer et al., 1997; Djordjevic et al., 2001; Greaves et al., 2007; Greaves et al., 2003b; Haines et al., 2009; Kosanovic et al., 2004; Kosanovic et al., 1997; Markovic et al., 2003; Markovic et al., 2006; Ohgushi et al., 2001; Peral and Iniguez, 2006; Ponyatovsky and Barkalov, 1992; Radulovic et al., 2010; Radulovic et al., 2013). Despite these efforts, little is known about the extent of Si-Al disorder and topological variations in both crystalline and amorphous phases during amorphization. Therefore, the objective of this study is to investigate the atomic structure and extent of chemical and topological disorders in both crystalline and amorphous phases during the temperature-induced amorphization of the synthetic zeolite, Na-zeolite A, using multi-nuclear solid-state NMR spectroscopy.

Na-zeolite A has been previously used as molecular sieves and catalysts (Cho et al., 2009; Mintova et al., 2001; Oliveira et al., 2009; Stucky et al., 1997). The structure of Na-zeolite A, as shown in Figure 1, consists of three secondary building units (SUBs) including α-cage, β-cage (sodalite cage), and double four-membered rings (D4R). The α-cage, with a diameter of 1.14 nm, is composed of eight-membered oxygen rings. The β-cage is located at each corner of the zeolite cube, and there exists a single six-membered ring (S6R) between the α-cage and β-cage. The double four-membered ring connects the two β-cages (Baerlocher et al., 2007). Water molecules are located inside the α- and β-cages of zeolite A (Baerlocher et al., 2007). With increasing temperature, the microporous Na-zeolite A network is expected to become relatively unstable and collapse into an amorphous phase at approximately 700-800 °C, followed by transformation into dehydrated crystalline phases (e.g., low-carnegieite and

nepheline) with further heating (Dimitrijevic et al., 2004; Greaves et al., 2007; Greaves et al., 2003b; Kosanovic et al., 2004; Mimura and Kanno, 1980; Stoch and Waclawska, 1994, and see references therein).

Previously, experimental studies have elucidated the nature of the temperature-induced amorphization of zeolites using X-ray diffraction (XRD), infrared spectroscopy (IR), and transmission electron microscopy (TEM) (Bursill and Thomas, 1981; Colyer et al., 1997; Dimitrijevic et al., 2004; Djordjevic et al., 2001; Flanigen et al., 1971; Greaves et al., 2007; Greaves et al., 2003a; Greaves et al., 2003b; Greaves and Meneau, 2004; Haines et al., 2009; Lutz et al., 1985; Markovic et al., 2003; Markovic et al., 2006; Radulovic et al., 2010; Radulovic et al., 2013). The previous IR studies of zeolites showed three distinct absorption bands of the sodalite family: internal asymmetric stretching vibrations, ν_{as} (T-O-T), between 800 and 1000 cm^{-1}; internal symmetric stretching vibrations, ν_s (T-O-T), between 500 and 800 cm^{-1}; and bending vibrations, δ (O-T-O), between 300 and 500 cm^{-1} (where T is the tetrahedral framework cation) (Henderson and Taylor, 1979). For Na-zeolite A, the characteristic vibrational bands of S6R and D4R were also observed over the range of 550-650 cm^{-1}; vibrations of D4R at 557 cm^{-1}, external vibrations of S6R at 623, 608, 578, 550 cm^{-1} (Djordjevic et al., 2001; Markovic et al., 2003; Markovic et al., 2006). These different vibration frequencies of the building units provide information on the temperature-induced changes in the building units in zeolite A, and the amorphization mechanism of Na-zeolite A has been proposed as follows (Djordjevic et al., 2001; Radulovic et al., 2013): dehydration of Na-zeolite A at ~ 400 °C induces the distortion of TO_4 frameworks. Furthermore, an increase in the temperature above 700 °C leads to a collapse of the long-range order in the zeolite (i.e., amorphization). During the amorphization, while the breaking of the O-O bond in the D4R structure is observed, the S6R building units do not collapse and the units are reconnected to form low-carnegieite (Dimitrijevic et al., 2004). Reconstructive phase transitions involving the breaking of linkages between Si and Al tetrahedrons are expected during the temperature-induced amorphization,

and subsequent crystallization at high temperatures (Greaves et al., 2003b). The remaining fundamental questions are the degree of chemical disorder (Si-Al ordering) during temperature-induced amorphization and transition.

The extent of Si-Al disorder in crystalline aluminosilicates including zeolites, mica, and feldspar have been studied for several decades (Carpenter, 1991; Cheng et al., 2000; Dirken et al., 1997; Dollase and Peacor, 1971; Herrero et al., 1985; Lee and Stebbins, 1999; Murdoch et al., 1988; Neuhoff et al., 2002a; Phillips et al., 1992; Stebbins et al., 1999b; Zhao et al., 2001, and see references therein). The short-range Si-Al order in the crystalline aluminosilicates is often described with Al avoidance i.e., Loewenstein's rule wherein the preference of the Al-O-Si linkage over the combination of Si-O-Si and Al-O-Al linkages is prevalent (Loewenstein, 1954). Unlike most of the crystalline analogs, the aluminosilicate glasses have been known to contain a non-negligible fraction of Al-O-Al with a Si-Al ratio of 1 (Lee and Stebbins, 1999; Lee and Stebbins, 2000b; Stebbins et al., 1999b). The extent of chemical disorder in the amorphous state of zeolite could influence the thermodynamic properties of the intermediate amorphous phase such as configurational heat capacity and entropy (Lee and Stebbins, 1999).

High-resolution solid-state NMR spectroscopy, which elucidates atomic structures around a specific nuclide of interest, has been effective in exploring the short-range structures (including Si-Al disorder) in diverse amorphous/disordered aluminosilicates (Carpenter, 1991; Cheng et al., 2000; Dollase and Peacor, 1971; Engelhardt and Michel, 1988; Hovis et al., 1992; Kim et al., 2010; Lee, 2005; Lee and Stebbins, 1999; Lee and Stebbins, 2000b; Lippmaa et al., 1980; Neuhoff et al., 2003; Phillips et al., 1992; Stebbins et al., 1986, and see references therein). Recent progress in 2D triple-quantum (3Q) MAS has resulted in considerably improved resolutions of the atomic configurations around quadrupolar nuclides such as ^{17}O and ^{27}Al in diverse crystalline and amorphous aluminosilicates (Lee, 2010, and references therein). Thus, this technique is suitable for estimating the temperature-induced changes in the degree of disorder in both amorphous and crystal phases during the amorphization of zeolite. Previous

133 solid-state NMR studies investigated the structures of zeolites before and after phase transitions
134 (e.g., Na-zeolite A and nepheline) (Dimitrijevic et al., 2004; Radulovic et al., 2013). However,
135 to the best of our knowledge, the atomic structures of the intermediate phases have not been
136 explored hitherto. ^{29}Si MAS NMR has been used to investigate the environment surrounding Si
137 atoms in zeolite, low-carnegieite, nepheline, and aluminosilicate glasses (Engelhardt and
138 Michel, 1988; Kirkpatrick, 1988; Lippmaa et al., 1980; Ramdas and Klinowski, 1984; Stebbins,
139 1988; Stebbins et al., 1986, and see references therein). The tetrahedral Si environment can be
140 conventionally described using the Q(*m*Al) notation, which refers to the tetrahedral Si groups
141 with *m* number of neighboring Al atoms. The width and shape of the ^{29}Si peak also provide the
142 topological information on a short range order: narrow peaks with full width at half maximum
143 (FWHM) of several ppm correspond to the crystalline phases while the broad peaks with
144 FWHM of several tens of ppm correspond to the amorphous phases in silicates (Engelhardt and
145 Michel, 1988). The ^{29}Si MAS NMR study of zeolites with increasing temperatures would
146 address the temperature-induced changes in Q(*m*Al) speciation. In addition, it would also help
147 to estimate the quantitative fraction of the amorphous phase during amorphization. Additionally,
148 ^{27}Al MAS NMR has been used to study the atomic configuration of aluminum atoms in
149 crystalline and amorphous aluminosilicates including zeolites (Engelhardt and Michel, 1988;
150 Lee, 2010; Lippmaa et al., 1986 and see references therein). In particular, 2D ^{27}Al 3QMAS
151 NMR successfully resolved crystallographically distinct aluminum sites in zeolite as well as
152 highly crystallized α-alumina and disordered γ-alumina (Chen et al., 2004; Hagaman et al.,
153 2010; Kim and Lee, 2013b; Neuhoff et al., 2002a; Sabarinathan et al., 2010). Thus, 2D ^{27}Al
154 3QMAS NMR is expected to resolve the multiple phases of aluminosilicates during the
155 temperature-induced amorphization. However, the 2D ^{27}Al 3QMAS NMR spectra of Na-zeolite
156 A and dehydrated phases have not been reported. Finally, we also determined that the degrees of
157 topological and chemical disorders could be directly explored by probing the atomic structures
158 around the oxygen atoms during the amorphization of zeolites using ^{17}O NMR (Lee, 2005; Lee

and Stebbins, 2000b). In particular, two-dimensional, solid-state ^{17}O 3QMAS NMR is a powerful tool to reveal the Si-Al ordering in crystalline and amorphous aluminosilicates by resolving the peaks of Si-O-Al, Si-O-Si, and Al-O-Al linkages (Amoureux et al., 1998; Ashbrook et al., 2002; Cheng et al., 2000; Dirken et al., 1997; Ernst et al., 2004; Freude et al., 2001; Lee et al., 2010; Lee and Stebbins, 2000b; Lee and Stebbins, 2009; Lee and Weiss, 2008; Lee et al., 2012; Neuhoff et al., 2002b; Pingel et al., 1998; Stebbins et al., 1997; Stebbins et al., 1999b; Zhao et al., 2001).

In this study, we explore the Si-Al ordering behavior in Na-zeolite A and its dehydrated crystalline phases at various temperatures using multi-nuclear solid-state NMR. Herein, we also report the first multi-nuclear (^{17}O, ^{29}Si, and ^{27}Al) NMR spectra of the intermediate amorphous phases during the temperature-induced phase transition of Na-zeolite A. Based on the NMR results, we attempt to provide insights into the detailed structural changes (chemical and topological) during the amorphization, and discuss the atomic-scale amorphization mechanism in zeolites. We explored the effect of temperature on the structural evolution of synthetic Na-zeolite A (Si/Al=1). Aluminosilicates with Si/Al = 1 would enable the estimation of the extent of Si-Al disorder unambiguously because the variation of Al-O-Al (and expected equal proportion of Si-O-Si) with varying Si-Al disorder is most sensitive at Si/Al = 1, ranging from 0 (complete Al avoidance) to 25 % (random distribution of Si-Al) (Lee and Stebbins, 1999). Because the Si/Al ratio in most of the natural zeolite is > 1, the estimation of Si-Al disorder in the networks, during amorphization, is not trivial. The current experimental results and methods with Na-zeolite A can be used to infer changes in the structural disorder in other diverse natural zeolite phases (see later section on implications).

EXPERIMENTAL METHODS

Sample preparation and characterization

Na-zeolite A (molecular sieves 4 Å from Sigma Aldrich, product no. 208604, chemical

185 composition of Na_2O: Al_2O_3: SiO_2 = 1:1:2.0±0.1 and additional H_2O molecules) was used. The
186 ground samples were sieved to separate the particles with diameters between 70 and 170 μm.
187 The zeolite particles were reacted with an equal weight of 40 % ^{17}O enriched H_2O in sealed gold
188 tubes at 150 °C and 0.5 kbar for 110 h in a cold seal vessel. The ^{17}O enriched zeolites were
189 annealed at different temperatures under Ar atmosphere. The annealing temperature of the
190 samples increased at the rate of 275 K/h to the target temperatures (e.g., 773 ~ 1373 K), and
191 further isothermal annealing was carried out for 3 h. We found that the rehydration of the
192 annealed samples at temperatures below 953 K resulted in the formation of initial zeolite phases
193 prior to annealing, which was consistent with the previous studies (Alberti et al., 2001; Bish and
194 Carey, 2001; Cruciani, 2006, and see references therein). Then, the annealed samples were
195 moved into a glove box (operated under Ar environment) wherein the samples were packed into
196 NMR rotors, and the NMR experiments were performed. The rehydration and related structural
197 changes in the samples were not observed during these experiments.
198
199 **X-ray diffraction**
200 The X-ray diffraction patterns of the samples were collected on a MiniFlex (Rigaku)
201 using Cu K_α X-rays, 2θ range of 5–70°, step width of 0.02°, and scan rate of 1°/min.
202
203 **NMR spectroscopy**
204 **^{29}Si NMR Spectroscopy** ^{29}Si MAS NMR spectra were collected on a Varian NMR spectrometer
205 (9.4 T) at a Larmor frequency of 79.55 MHz (4 mm Doty probe) and spinning speed of 11 kHz.
206 A single-pulse sequence with an approximately 30° pulse (1.6 μs) and a delay time of 120 s was
207 used. TMS was used as an external reference.
208 **^{27}Al NMR spectroscopy** ^{27}Al MAS spectra were collected on a Varian NMR (9.4 T)
209 spectrometer with a Doty 4 mm probe. The single-pulse acquisition with a pulse length of 0.2 μs
210 [radio frequency (*rf*) tip angle of about 15° for solids] was used with a recycle delay of 1 s and

spinning speed of 15 kHz. ^{27}Al 3QMAS NMR spectra were collected using fast amplitude modulation- (FAM-) based shifted-echo pulse sequences (1 s relaxation delay - 3.0 μs pulse for 3Q excitation–t_1 delay–FAM pulse train with a 0.8 μs pulse-echo delay - 19 μs soft pulse for echo reconversion–t_2 acquisition) (Baltisberger et al., 1996; Madhu et al., 1999; Zhao et al., 2001). A solution of $AlCl_3$ (2 mol%) was used as an external standard.

^{17}O NMR spectroscopy ^{17}O NMR spectra of amorphous silica gel were collected on a Varian NMR spectrometer of 9.4 T at a Larmor frequency of 54.23 MHz (Doty 4 mm probe) and a spinning speed of 15 kHz. ^{17}O 3QMAS NMR spectra were collected using FAM-based shifted-echo pulse sequences (1 s relaxation delay - 3.0 μs pulse for 3Q excitation–t_1 delay–FAM pulse train with a 0.8 μs pulse-echo delay - 19 μs soft pulse for echo reconversion–t_2 acquisition) (Baltisberger et al., 1996; Madhu et al., 1999; Zhao et al., 2001). Tab water was used as an external standard.

RESULTS AND DISCUSSION

XRD patterns of Na-zeolite A

Previous XRD studies have reported the temperature-induced phase transformation sequences of Na-zeolite A → amorphous phase → low-carnegieite between 973 K and 1123 K and low-carnegieite → nepheline above 1173 K (Kosanovic et al., 2004; Lutz et al., 1985). The detailed transformation temperatures varied while the pure amorphous phase was not often retained during the temperature-induced phase transition of Na-zeolite A, which depended on the heating rate, isothermal heating duration, heating media (e.g., air, Ar, water vapor), and framework Si/Al ratio (Cruciani, 2006; Dimitrijevic et al., 2004; Greaves et al., 2003b; Lutz et al., 1985; Markovic et al., 2003; Radulovic et al., 2013). For instance, the amorphization temperature for zeolites tends to increase with increasing heating rate and Si/Al ratio (Cruciani, 2006; Greaves et al., 2003b). Thus, we measured the XRD patterns to identify the crystalline and amorphous phases in the samples, and phase transition temperatures in the current study.

Figure 1 shows the XRD patterns of Na-zeolite A and its dehydrated phases with increasing annealing temperature, and confirms the crystalline and amorphous phases of Na-zeolite A and dehydrated phases after annealing. The diffraction patterns of Na-zeolite A were observed at temperatures over the range of 298 K - 953 K. The intensities of the diffraction peaks for (200) (220) (222) reflections increased with increasing temperature from 773 K to 933 K compared to those of the other diffraction peaks. These results were reported in the previous studies and might be attributed to the dehydration and/or accompanying migration of sodium ions (Breck et al., 1956; Pilter et al., 2000; Reed and Breck, 1956). At 953 K, the overall intensities of the diffraction patterns of Na-zeolite A apparently decreased, thereby indicating the onset of the phase transition of Na-zeolite A→ amorphous phase. At 973 K, sharp diffraction peaks with low intensities for the low-carnegieite phase are observed. These results suggest that the Na-zeolite A networks collapse into an amorphous phase between ~873 K and ~953 K while the amorphous phase re-crystalizes into low-carnegieite between ~ 953 K and ~ 973 K. The proportion of the amorphous phases in the sample reaches its maximum between 953 K and 973 K although the pure amorphous phase is not observed in this study. With a further increase in the annealing temperature (1073 ~ 1173 K), low-carnegieite transforms into nepheline.

^{29}Si MAS NMR results and analysis: Temperature-induced changes in silicon environments

Figure 2 shows the ^{29}Si MAS NMR spectra of Na-zeolite A and its dehydrated phases with increasing annealing temperatures. In the ^{29}Si MAS NMR spectra of Na-zeolite A at 298 K (i.e., before annealing), a narrow peak corresponding to the tetrahedral Si site with four neighboring Al atoms [i.e., Q(4Al)] and small feature of Q(3Al) are observed at -88 ppm and -92 ppm, respectively (Engelhardt and Michel, 1988; Lippmaa et al., 1981). At 873 K, the peak width for Q(4Al) species at -88 ppm slightly increases, indicating an increase in the topological disorder around the Si tetrahedron in the crystalline zeolite network. The intensity ratio of Q(4Al):Q(3Al) in the Na-zeolite A at 298 K and 873 K is 91±2:9±2, thereby indicating that Si/Al

263 = 1.02±0.10. At 953 K, a broad Gaussian-shaped peak ranging from -80 to -100 ppm and narrow
264 peak at -88 ppm are observed. While the position of the broad peak in the spectrum for the
265 dehydrated sample at 973 K is apparently invariable, the narrow peak at -88 ppm disappears.
266 Instead, the peak at -82 ppm is observed at 973 K. We assigned the broad peak to the Si atoms in
267 the amorphous phase (Maekawa et al., 1991). The narrow peak at -82 ppm is assigned to the
268 Q(4Al) environment in low-carnegieite based on the previous ^{29}Si MAS NMR studies (Stebbins
269 et al., 1986; Thompson et al., 1993). These results are consistent with the XRD results, wherein
270 the formation of low-carnegieite is observed at 953 - 973 K (Figure 1). At 1073 K, the spectrum
271 shows two narrow peaks at -82 ppm and -88 ppm for Q(4Al) species and one broad peak at
272 approximately -87 ppm: these peaks represent the Si environments in low-carnegieite (one peak
273 at -82 ppm), nepheline (two peaks at -82 ppm and -88 ppm), and possibly amorphous phase
274 (broad peak), respectively. At 1173 K, where the nepheline is the single crystalline phase
275 according to XRD result, two sharp peaks at -82 ppm and -88 ppm, which are assigned to
276 crystallographically distinct Q(4Al) sites (Si2 and Si1, respectively), and a broad peak at ~ -94
277 ppm, tentatively assigned to the Q(3Al) site, are also observed (Gregorkiewitz, 1984; Stebbins et
278 al., 1986). The Q(3Al) peak in the ^{29}Si MAS NMR spectrum for the dehydrated sample at 1173
279 K might be attributed to the Si/Al ratio of 1.02±0.1. Previous studies have also showed that the
280 Q(3Al) peak was observed in the ^{29}Si MAS NMR spectrum for the natural nepheline containing
281 excess Si (Si/Al=1.07) (Stebbins et al., 1986). Otherwise, the amorphous phases might exist even
282 at 1173 K and affect the peak shapes in the ^{29}Si MAS NMR spectrum.

283 In order to quantify the proportions of Na-zeolite A and dehydrated phases at various
284 annealing temperatures, the ^{29}Si MAS NMR spectra are simulated with several Gaussian
285 functions representing Q(*m*Al) species in the multi-crystalline and amorphous phases in the
286 samples (Figure 3). Notably, the simulation results of ^{29}Si MAS NMR spectra in this study are
287 semi-quantitative and contained potential uncertainties. The peak position and width of the Q
288 species except the Q(4Al) species in Na-zeolite A were fixed: although the simulation of the

spectrum with such fixed variables might reduce the overall quality of the fit with the experimental result, this could also remove the potential lack of generalization in the trends observed for the spectra. Q(4Al), Q(3Al) in Na-zeolite A (-88 ppm and -92 ppm, respectively) and low-carnegieite (-82 ppm) peaks were simulated using a single Gaussian function. The Q(*m*Al) species in the amorphous phase were simulated using one Gaussian function with FWHM of 13.9 ppm. The two Q(4Al) peaks for Si2, Si1 tetrahedral sites and one Q(3Al) peak in nepheline were simulated with three Gaussian functions at -83, -88, and -93 ppm, respectively. At 1073 K, the Q(4Al) species in low-carnegieite and Si2 site in nepheline were simulated using a single Gaussian function because their peak positions were identical. A1173 K, the relatively weak features of the amorphous phases might be present, as indicated by the presence of the intensities at both low and high frequency ranges around the sharp crystalline peaks. The peak width of the Q(4Al) species in Na-zeolite A at 873 K was slightly larger than that at 298 K owing to an increase in the structural distortion of the Si tetrahedron. The simulation results show that the amorphous phase coexists with low-carnegieite and nepheline up to 1073 K (possibly, even at 1173 K). Although further kinetic studies are certainly necessary, the prevalence of amorphous phases at ~1073 K implies that the phase transition from the amorphous to crystalline phase such as low-carnegieite and nepheline is rather sluggish.

^{27}Al MAS NMR results and analysis: Temperature-induced changes in Al environments

Figure 4 shows the ^{27}Al MAS NMR spectra of Na-zeolite A and dehydrated phases at 9.4 T with increasing annealing temperature. The spectra highlights the resolved $^{[4]}$Al sites in multiple phases including Na-zeolite A, low-carnegieite, nepheline, and the amorphous phase (Corbin et al., 1984; Hovis et al., 1992; Lippmaa et al., 1986). At 298 K, the narrow $^{[4]}$Al peak for Na-zeolite is observed at 59 ppm (Lippmaa et al., 1986). The FWHM of the $^{[4]}$Al peak of Na-zeolite decreases from 3.5 ppm at 298 K to 2.9 ppm at 773 K, indicating that the topological disorder decreases after annealing at 773 K. At 823 K, the peak width and position suddenly

vary: FWHM significantly increases to 9.7 ppm from 2.9 ppm at 773 K and its position also shifts to a low frequencies. The observed change in the peak position and width might be owing to an increase in the topological disorder, indicating a distortion in the frameworks in Na-zeolite A upon dehydration between 773 K and 823 K (Lippmaa et al., 1986). The broad $^{[4]}$Al peak between 823 K and 953 K readily reverted back to the original narrow peak before annealing, upon rehydration under ambient atmosphere (see below section on reversibility of temperature-induced phase transition of Na-zeolite A). At 953 K, an additional broad peak approximately over the range of 30 - 80 ppm is observed, and tentatively assigned to the amorphous phase based on previous ^{27}Al NMR studies on Na-aluminosilicate glasses (Lee and Stebbins, 2000b; Neuville et al., 2006). At 973 K, the width of the $^{[4]}$Al peak at 58 ppm is narrower than that at 953 K, indicating a phase transformation from the amorphous phase to low-carnegieite. At 1073 K, two peaks are observed at 64 ppm and 59 ppm, which are assigned to two crystallographically distinct $^{[4]}$Al sites in nepheline, based on the previous ^{27}Al NMR studies on nepheline (Hovis et al., 1992; Lippmaa et al., 1986).

Figure 5 shows the ^{27}Al 3QMAS NMR spectra at 9.4 T of Na-zeolite A and dehydrated phases with increasing annealing temperature. The $^{[4]}$Al peak of Na-zeolite A is observed at -33 ppm and 58 ppm in isotropic and MAS dimension, respectively. The $^{[4]}$Al peak at 873 K shows a broad peak shape, which was similar to that of Na-zeolite A before annealing, suggesting an increase in the topological disorder around the Al tetrahedron of the Na-zeolite A. At 953 K and 973 K, a broad $^{[4]}$Al peak corresponding to the Al sites in the amorphous phase is observed (Lee and Stebbins, 2000b). At 1073 K and 1173 K, crystallographically distinct $^{[4]}$Al sites of nepheline and low-carnegieite are observed. The total isotropic projection, which is the sum over data along lines parallel to MAS dimension, is also shown in Figure 6, wherein the $^{[4]}$Al sites in the crystalline and amorphous phases were resolved in the isotropic dimension. Because the isotropic dimension in the 3QMAS NMR spectra is free from quadrupolar broadening, the Al sites in the distorted zeolite frameworks and amorphous phase were distinguished in the isotropic

dimension. The peak width of the $^{[4]}$Al peak in Na-zeolite A slightly increases from 2.5 ppm at 298 K to 4.7 ppm at 873 K. The broad amorphous peak over the range of -30 - -50 ppm is observed at 933 - 973 K. The proportion of the amorphous phase is maximized at ~ 973 K, which is consistent with the ^{29}Si MAS NMR results (Figure 3).

Comparison of ^{29}Si and ^{27}Al MAS NMR spectra

The detailed changes in the zeolite frameworks upon annealing could be obtained by comparing the results of the ^{29}Si NMR and ^{27}Al NMR spectra, allowing us to distinguish the degree of distortion in Si and Al tetrahedrons. Figure 7 shows the comparison of ^{29}Si and ^{27}Al MAS NMR spectra at 298 K and 873 K, respectively, highlighting the different peak broadening between ^{29}Si and ^{27}Al MAS NMR spectra. The Q(4Al) peak in the ^{29}Si MAS NMR spectra shows slight changes in the peak position and width before and after annealing at 873 K. The peak positions are identical in both instances while the FWHM changes from 1.7 ppm at 298 K and to 2.8 ppm at 873 K. The $^{[4]}$Al peak in the ^{27}Al NMR spectra, otherwise, shows significant changes before and after annealing at 873 K. The peak position shifts to a lower frequency from 59 ppm at 298 K to 54 ppm at 873 K, while the FWHM changes from 3.5 ppm at 298 K to 9.7 ppm at 873 K. Previous studies have indicated that the ^{29}Si and ^{27}Al chemical shifts of zeolites had linear correlations with mean Si-O-Al bond angles, which equally affects the peak position and width in the ^{29}Si and ^{27}Al NMR spectra (Engelhardt and Michel, 1988; Lippmaa et al., 1986; Newsam, 1987). Thus, the variation in the Si-O-Al bond angle may not cause the significant peak broadening in the ^{27}Al MAS NMR spectra as was the case with ^{29}Si MAS NMR. The peak broadening of the $^{[4]}$Al peak in the ^{27}Al MAS NMR spectra might be prominent because the ^{27}Al is a quadrupolar nuclide. A quadrupolar coupling constant (C_q), an important NMR parameter affecting the peak width and shape in ^{27}Al MAS NMR spectra, is an index of the degree of distortion around an Al tetrahedron (Engelhardt and Michel, 1988; Engelhardt and Veeman, 1993; Weller et al., 1994). The C_q values of $^{[4]}$Al site in Na-zeolite A at 298 K and 873 K,

367 calculated from the center of gravity in 2D ^{27}Al 3QMAS NMR spectra, were 1.4-1.6 MHz and
368 2.4-2.8 MHz, respectively, depending on the value of the asymmetry parameter (η) ($0 \leq \eta \leq 1$).
369 These results indicate that C_q in $^{[4]}$Al site in Na-zeolite A increases with increasing temperature
370 from 298 K to 873 K. Therefore, a small structural variation in the zeolite framework would lead
371 to a distribution of the chemical shifts and C_q for $^{[4]}$Al peak in ^{27}Al NMR spectra, whereas it
372 would only affect the distribution of the chemical shifts in ^{29}Si NMR spectra.
373
374 **^{17}O MAS NMR results and analysis: Temperature-induced changes in oxygen**
375 **environments**
376 Figure 8 shows the ^{17}O 3QMAS NMR spectra of Na-zeolite A and dehydrated phases
377 with increasing annealing temperature, highlighting the temperature-induced structural changes
378 in the oxygen environments. Na-zeolite A has three crystallographically distinct O atom sites, O1,
379 O2, and O3 (Freude et al., 2001). O1 is the oxygen linking the adjacent sodalite units, while O2
380 and O3 form the 4-membered rings and 6-membered rings in the sodalite cage (i.e., β-cage), as
381 shown in Figure 1 (Baerlocher et al., 2007). At 298 K, crystallographically distinct Si-O-Al sites
382 including O1, O2, and O3 in Na-zeolite A are partially resolved in the isotropic dimension: the
383 peaks at -25 ppm and -31 ppm were assigned to Si-O2-Al linkage and unresolved Si-O1-Al and
384 Si-O3-Al linkages, respectively, according to previous studies (Neuhoff et al., 2002b; Pingel et
385 al., 1998). Previous works have reported the NMR parameters for O1, O2, and O3 sites in Na-
386 zeolite A based on the differences in their Si-O-Al angles and population ratios: the Si-O-Al
387 bond angles are 145.6°, 159.5°, and 147.6° for O1, O2, and O3 sites while the population ratio
388 O1:O2:O3 is 1:1:2 (Gramlich and Meier, 1971; Neuhoff et al., 2002b; Pingel et al., 1998).
389 Approximately, 2 % of the oxygen population is expected to be in the form of Si-O-Si according
390 to ^{29}Si MAS NMR results: the peak for Si-O-Si is not prominently observed because the 3Q
391 excitation efficiency of Si-O-Si is lower than that of Si-O-Al in the 3QMAS experiments (Lee
392 and Stebbins, 2000a; Xu and Stebbins, 1998). After annealing at 873 K, the three Si-O-Al sites

393 are not resolved because of peak broadening in the MAS and isotropic dimensions, indicating an
394 increase in the topological disorder around the oxygen atoms. Note that the temperature-induced
395 amorphization does not occur at 873 K, as shown in ^{29}Si MAS NMR spectra (Figure 2 and 3).
396 Between 933 K and 973 K, the ^{17}O 3QMAS NMR spectra show three types of bridging oxygen
397 atoms (BO, e.g., Si-O-Al, Al-O-Al, and Si-O-Si). The peaks at ~ -12 ppm, -25 ppm, and -45 ppm
398 in the isotropic dimension correspond to Al-O-Al, Si-O-Al, and Si-O-Si linkages, respectively at
399 9.4 T (Lee and Stebbins, 2000b; Stebbins et al., 1999a). The crystallographically distinct Si-O-Al
400 sites such as O1, O2, and O3 are not distinguished in the ^{17}O 3QMAS NMR spectra at 933 ~ 973
401 K due to an increased disorder. As indicated by the change in the number of contour lines of the
402 Al-O-Al peak, the proportion of Al-O-Al and Si-O-Si linkages has a maximum at 953 K,
403 indicating that the degree of chemical disorder between Al and Si in the Na-zeolite A is
404 maximized with amorphization. We found that the XRD pattern did not show a significant
405 evidence of amorphization for the dehydrated Na-zeolite A at 933 K (see Figure 1), whereas the
406 Al-O-Al linkage was seen in the ^{17}O NMR spectra for the same sample. These results suggests
407 that a small proportion of the amorphous phase in zeolites was not well-distinguished using XRD
408 alone. At 1073 K, the peak intensities of the Al-O-Al and Si-O-Si linkage were still observed,
409 though with small intensity, thereby implying that the amorphous phase exists. At 1173 K, the Si-
410 O-Al peak is observed, which could be assigned to the oxygen sites in nepheline, in accordance
411 to the XRD results. While it has been known that crystallographically distinct six oxygen sites
412 (from O1 to O6 depending on bond angle and neighboring tetrahedral sites) exist in nepheline,
413 these are not resolved well in the ^{17}O 3QMAS NMR spectrum at 9.4 T (Buerger et al., 1954).
414 Figure 9(a) shows the total isotropic projections of the ^{17}O 3QMAS NMR spectra for the
415 Na-zeolite A and dehydrated phases, confirming that Si-O-Al is dominant, and small but non-
416 negligible fractions of Al-O-Al and Si-O-Si are also detected at 933 - 1073 K. These results
417 indicate that the chemical order between Si and Al is affected by amorphization. Figure 9(b)
418 depicts the magnified spectra of the projections in the isotropic dimension of the ^{17}O 3QMAS

NMR spectra of Na-zeolite A and dehydrated phases over the frequency range of -15 - -45 ppm, thereby highlighting the changes in the structural disorder around the Si-O-Al linkage during amorphization. At 298 K, the peaks for O1 and O3 species overlaps with each other, while the peak for O2 species is resolved at -24 ppm in the isotropic dimension. With increasing temperature up to 873 K, the peaks for the distinct oxygen environments broaden and shift to higher frequency in the isotropic dimension. The shift in the peak positions of Si-O-Al linkages in Na-zeolite A might be due to the removal of H_2O and/or migration of Na ions upon annealing as the ^{17}O chemical shift of the Na-zeolite A was affected by the extra framework species (e.g., water molecules and cations) as well as Si-O-Al bond angle (Neuhoff et al., 2002b). Over the temperature range of 933 K - 1073 K, Al-O-Al and Si-O-Si as well as Si-O-Al linkages were observed while the peaks for Al-O-Al and Si-O-Si linkages were not observed at 1173 K. Previous studies on the temperature-induced phase transition of Na-zeolite A have reported that the breaking of Si-O-Al bridges in zeolite A started within D4R units while the α- and β-cage units were retained through the collapse of the zeolite frame works (Bursill and Thomas, 1981; Djordjevic et al., 2001). In this study, the crystallographically distinct three Si-O-Al linkages (i.e., O1, O2, and O3 sites) are partially resolved for Na-zeolite A at 298 K and 873 K. However, these are not significantly resolved between 933 K and 1073 K, indicating that the β-cage units might possess highly distorted structures. Thus, the two types of Si-O-Al linkages (O2 and O3 sites) in the β-cage could not be distinguished during amorphization.

Reversibility of temperature-induced phase transition of Na-zeolite A

The dehydrated zeolites without the collapse of frameworks are known to be readily rehydrated (i.e., reversible dehydration), whereas the completely dehydrated zeolite with subsequent amorphization do not undergo rehydration (i.e., irreversible dehydration) (Alberti et al., 2001; Bish and Carey, 2001; Cruciani, 2006, and references therein). The structure of dehydrated zeolites without amorphization may be readily revert to the structure of hydrated

zeolite. The combination of sample packing into NMR rotors under Ar atmosphere in a glove box and measurement of NMR spectrum during spinning of the sample often prevent the rehydration of the dehydrated sample (Kim and Lee, 2013a).

Figure 10 shows the effect of the sample rehydration on the ^{27}Al MAS NMR spectra of the dehydrated Na-zeolite A at 873 K: the black and red lines indicate the spectra of the samples packed in a glove box (under Ar gas) and an open atmosphere, respectively. We note that the exposure time to atmosphere (i.e., a time for sample packing in an open atmosphere) was only a few minutes. The spectra show obvious structural changes in the dehydrated samples upon exposure to an open atmosphere (i.e., rehydration), while the black line shows the broad peak shape at ~ 54 ppm, the red line shows a rather sharp peak at 59 ppm. The peak shape and position of the $^{[4]}$Al peak in rehydrated samples (red line) are similar to those in Na-zeolite A before annealing. These results indicate that the dehydrated structure of Na-zeolite A could experience rehydration with exposure to atmosphere for only a few-minutes, and the slight distortion of the zeolite framework with annealing below 873 K might go undetected without careful sample handling. All the samples for NMR experiments in this work were packed under Ar gas in a glove box, and rehydration did not occur.

Figure 11 shows the ^{17}O 3QMAS NMR spectra of the dehydrated Na-zeolite A at 933 K (top) and the spectrum collected for the same sample after 7 months (stored in a desiccator) (bottom). The three peaks for Al-O-Al and Si-O-Si as well as Si-O-Al linkages are observed in the ^{17}O 3QMAS NMR spectra of the dehydrated Na-zeolite A at 933 K, suggesting the collapse of the zeolite framework, and the formation of the amorphous phases. However, the spectrum collected after 7 months does not show the Al-O-Al and Si-O-Si linkages. The peak shape corresponding to the Si-O-Al linkage is similar to that before annealing. These results indicate that the collapsed framework in the dehydrated Na-zeolite A at 933 K could be restored back to the zeolite framework upon rehydration, which is consistent with the results of the previous studies. Additionally, the results indicates that the rehydration of the intermediate amorphous

phase might lead to the formation of crystalline phases (Alberti et al., 2001; Bish and Carey, 2001; Cruciani, 2006, and references therein). We found that the rehydration of the dehydrated Na-zeolite A at 933 K was not well-distinguished using XRD partly because of the low proportion of the amorphous phase in the sample (see section for O-17 NMR results above). Further experimental efforts would be necessary to confirm the observed trend in transitions involving the amorphous phases.

Implications: Si-Al ordering in crystalline and amorphous aluminosilicates during temperature-induced amorphization

Based on the high-resolution solid-state NMR results, we investigated the structural changes (chemical and topological) during the amorphization of Na-zeolite A. While several previous studies have reported the temperature-induced phase transition in natural/synthetic zeolites (Bish and Carey, 2001; Cruciani, 2006; Dimitrijevic et al., 2004), the Si-Al ordering behavior in the intermediate amorphous phase upon heating has not been reported hitherto. With increasing annealing temperatures up to 873 K, a topological disorder in the zeolite frameworks was observed, as evidenced by an increase in the widths of $^{[4]}$Al and Q(4Al) peaks in the ^{27}Al and ^{29}Si MAS NMR spectra of Na-zeolite A, and complete Si-Al ordering with respect to chemical disorder. These collapsed structures of zeolite frameworks reverted to their forms before annealing with exposure to the open atmosphere for only a few minutes (i.e., reversible changes). With further increase in the annealing temperature from 873 K up to 973 K, the amorphization of zeolite frameworks occurred with the accompanying T-O-T bond breaking. Both topological and chemical disorders were observed in the amorphous phase in Na-zeolite A as evidenced by the presence of Al-O-Al, Si-O-Si peaks as well as Si-O-Al peak in the ^{17}O 3QMAS NMR spectra, and the broad peak shapes in ^{29}Si and ^{27}Al NMR spectra. Finally, at temperatures above ~ 1073 K, the phase transition of amorphous phase → low-carnegieite → nepheline occurred with a decrease in both topological and chemical disorders (i.e., intensity of

Al-O-Al and Si-O-Si linkages in ^{17}O 3QMAS NMR spectra). The observed structural changes in Na-zeolite A and other dehydrated phases suggested that the amorphization of zeolites was accompanied by increases in both topological and chemical disorders in the intermediate amorphous phase.

Temperature-induced transitions of natural zeolite occur during diagenesis with the increase of burial depth and/or metamorphism by intrusion of plutonic mass (Utada, 2001 and references therein). Diverse experiments have shown that natural zeolites including natrolite and analcime undergo amorphization during thermal phase transitions (Abe et al., 1973; Arletti et al., 2006; Bish and Carey, 2001; Danisi et al., 2012; Fischer et al., 2008; Ori et al., 2009; Park et al., 2013, and references therein). The atomic structure of the intermediate phase of zeolites during phase transition, however, is not fully understood. The current experimental results and methods involving model zeolite phases with Si/Al = 1 can be employed to infer the changes in structural disorder and configurational entropy due to Si-Al mixing in other diverse natural zeolite phases (with Si/Al > 1) such as natrolite ($Na_{16}Al_{16}Si_{24}O_{80}\cdot 16H_2O$), analcime ($Na_{16}Al_{16}Si_{32}O_{96}\cdot 16H_2O$), and faujasite ($Na_{20}Ca_{12}Mg_8Al_{60}Si_{32}O_{384}\cdot 235H_2O$) as an increase in the chemical disorder in the intermediate amorphous phase of zeolites would be expected, regardless of the Si/Al ratio. The systematic effect of temperature, heating rate, chemical composition and network topology on the changes in structural disorder in natural zeolites and the intermediate phases remains to be established.

ACKNOWLEDGMENT

This research was supported by the Korean Science and Engineering Foundation grants through the National Research Laboratory Program (NRF-2012R1A2A1A05026411). We thank Prof. Greaves for his helpful discussion. We appreciate the constructive and helpful suggestions of the three anonymous reviewers.

REFERENCES CITED

Abe, H., Aoki, M., and Konno, H. (1973) Synthesis of analcime from volcanic sediments in sodium silicate solution. Contributions to Mineralogy and Petrology, 42, 81-92.

Alberti, A., Vezzalini, G., Quartieri, S., Cruciani, G., and Bordiga, S. (2001) Rehydration mechanisms in zeolites: reversibility of T-O-T breaking and of tetrahedral cation migration in brewsterite. Microporous and Mesoporous Materials, 42, 277-287.

Arletti, R., Mazzucato, E., and Vezzalini, G. (2006) Influence of dehydration kinetics on T-O-T bridge breaking in zeolites with framework type STI: The case of stellerite. American Mineralogist, 91, 628-634.

Amoureux, J.P., Bauer, F., Ernst, H., Fernandez, C., Freude, D., Michel, D., and Pingel, U.T. (1998) ^{17}O multiple-quantum and ^{1}H MAS NMR studies of zeolite ZSM-5. Chemical Physics Letters, 285, 10-14.

Ashbrook, S.E., Berry, A.J., and Wimperis, S. (2002) ^{17}O multiple-quantum MAS NMR study of pyroxenes. The Journal of Physical Chemistry B, 106, 773-778.

Baerlocher, C., McCusker, L.B., and Olson, D.H. (2007) Atlas of zeolite framework types, 6th edition. Elsevier, Amsterdam, Netherlands.

Baltisberger, J.H., Xu, Z., Stebbins, J.F., Wang, S.H., and Pines, A. (1996) Triple-quantum two-dimensional ^{27}Al magic-angle spinning nuclear magnetic resonance spectroscopic study of aluminosilicate and aluminate crystals and glasses. Journal of the American Chemical Society, 118, 7209-7214.

Bish, D.L., and Carey, J.W. (2001) Thermal behavior of natural zeolites. In D.L. Bish, and D.W. Ming, Eds., Natural zeolites: occurrence, properties, applications, 45, p. 403-452. Reviews in Mineralogy and Geochemistry, Mineralogical Society of America, Chantilly, Virginia.

Boyd, G.E., Adamson, A.W., and Myers, L.S. (1947) The exchange adsroption of ions from

549 aqueous solutions by organic zeolite. II. Kinetics. Journal of the American Chemical
550 Society, 69, 2836-2848.
551 Breck, D.W., Eversole, W.G., Milton, R.M., Reed, T.B., and Thomas, T.L. (1956) Crystalline
552 zeolites.1. The properties of a new synthetic zeolite, type A. Journal of the American
553 Chemical Society, 78, 5963-5971.
554 Buerger, M.J., Klein, G.E., and Donnay, G. (1954) Determination of the crystal structure of
555 nepheline. American Mineralogist, 39, 805-818.
556 Bursill, L.A., and Thomas, J.M. (1981) High-resolution electron microscopy of microcrystalline,
557 partially crystalline, and amorphous silicates. The Journal of Physical Chemistry, 85,
558 3007-3010.
559 Carpenter, M.A. (1991) Mechanisms and kinetics of Al-Si ordering in anorthite 2. Energetics and
560 a ginzburg-landau rate law. American Mineralogist, 76, 1120-1133.
561 Chen, J.X., Chen, T.H., Guan, N.J., and Wang, J.Z. (2004) Dealumination process of zeolite
562 omega monitored by ^{27}Al 3QMAS NMR spectroscopy. Catalysis Today, 93-95, 627-630.
563 Cheng, X., Zhao, P.D., and Stebbins, J.F. (2000) Solid state NMR study of oxygen site exchange
564 and Al-O-Al site concentration in analcime. American Mineralogist, 85, 1030-1037.
565 Cho, K., Cho, H.S., de Ménorval, L.-C., and Ryoo, R. (2009) Generation of mesoporosity in LTA
566 zeolites by organosilane surfactant for rapid molecular transport in catalytic application.
567 Chemistry of Materials, 21, 5664-5673.
568 Colyer, L.M., Greaves, G.N., Carr, S.W., and Fox, K.K. (1997) Collapse and recrystallization
569 processes in zinc-exchanged zeolite-A: A combined X-ray diffraction, XAFS, and NMR
570 study. The Journal of Physical Chemistry B, 101, 10105-10114.
571 Corbin, D.R., Farlee, R.D., and Stucky, G.D. (1984) The framework chemistry of zeolites: ^{27}Al
572 MAS NMR of extralattice tetrahedral aluminum species. Inorganic Chemistry, 23, 2920-
573 2922.
574 Coronas, J., and Santamaria, J. (2004) The use of zeolite films in small-scale and micro-scale

applications. Chemical Engineering Science, 59, 4879-4885.

Cruciani, G. (2006) Zeolites upon heating: Factors governing their thermal stability and structural changes. Journal of Physics and Chemistry of Solids, 67, 1973-1994.

Danisi, R.M., Armbruster, T., and Lazic, B. (2012) In situ dehydration behavior of zeolite-like cavansite: A single-crystal X-ray study. American Mineralogist, 97, 1874-1880.

Dimitrijevic, R., Dondur, V., Vulic, P., Markovic, S., and Macura, S. (2004) Structural characterization of pure Na-nephelines synthesized by zeolite conversion route. Journal of Physics and Chemistry of Solids, 65, 1623-1633.

Dirken, P.J., Kohn, S.C., Smith, M.E., and vanEck, E.R.H. (1997) Complete resolution of Si-O-Si and Si-O-Al fragments in an aluminosilicate glass by ^{17}O multiple quantum magic angle spinning NMR spectroscopy. Chemical Physics Letters, 266, 568-574.

Djordjevic, J., Dondur, V., Dimitrijevic, R., and Kremenovic, A. (2001) Structural investigations of celsian glass derived from Ba-LTA zeolite. Physical Chemistry Chemical Physics, 3, 1560-1565.

Dollase, W.A., and Peacor, D.R. (1971) Si-Al ordering in nephelines. Contributions to Mineralogy and Petrology, 30, 129-134.

Engelhardt, G., and Michel, D. (1988) High-resolution solid-state NMR of silicates and zeolites, 485 p. Wiley, New York

Engelhardt, G., and Veeman, W. (1993) Assignment of the ^{27}Al and ^{31}P NMR spectra of the aluminophosphate molecular sieve VPI-5. Journal of the Chemical Society, Chemical Communications, 622-623.

Ernst, H., Freude, D., Kanellopoulos, J., Loeser, T., Prochnow, D., and Schneider, D. (2004) Has ^{17}O NMR been established as a spectroscopic tool for zeolite characterization? In E. VanSteen, M. Claeys, and L.H. Callanan, Eds., Recent advances in the science and technology of zeolites and related materials, 154, p. 1173-1179. Elsevier, Amsterdam, Netherlands.

601 Fischer, R.X., Kahlenberg, V., Lengauer, C.L., and Tillmanns, E. (2008) Thermal behavior and
602 structural transformation in the chabazite-type zeolite willhendersonite,
603 $KCaAl_3Si_3O_{12}\cdot 5H_2O$. American Mineralogist, 93, 1317-1325.
604 Flanigen, E.M., Khatami, H., and Szymansk.Ha. (1971) Infrared structural studies of zeolite
605 frameworks. In E.M. Flanigen, and L.B. Sand, Eds., Molecular Sieve Zeolites-I, 101, p.
606 201-229. American Chemical Society, Washington, D.C.
607 Freude, D., Loeser, T., Michel, D., Pingel, U., and Prochnow, D. (2001) ^{17}O NMR studies of low
608 silicate zeolites. Solid State Nuclear Magnetic Resonance, 20, 46-60.
609 Gramlich, V., and Meier, W.M. (1971) The crystal structure of hydrated Na A: A detailed
610 refinement of a pseudosymmetric zeolite structure. Zeitschrift fu□r Kristallographie,
611 Kristallgeometrie, Kristallphysik, Kristallchemie, 133, 134-149.
612 Greaves, G.N., Meneau, F., Kargl, F., Ward, D., Holliman, P., and Albergamo, F. (2007) Zeolite
613 collapse and polyamorphism. Journal of Physics: Condensed Matter, 19, 415102
614 Greaves, G.N., Meneau, F., Majerus, O., Jones, D.G., and Taylor, J. (2005) Identifying vibrations
615 that destabilize crystals and characterize the glassy state. Science, 308, 1299-1302.
616 Greaves, G.N., Meneau, F., and Sankar, G. (2003a) SAXS/WAXS and XAFS studies of zeolite
617 stability. Nuclear Instruments and Methods in Physics Research Section B: Beam
618 Interactions with Materials and Atoms, 199, 98-105.
619 Greaves, G.N., Meneau, F., Sapelkin, A., Colyer, L.M., Gwynn, I.A., Wade, S., and Sankar, G.
620 (2003b) The rheology of collapsing zeolites amorphized by temperature and pressure.
621 Nature Materials, 2, 622-629.
622 Greaves, N., and Meneau, F. (2004) Probing the dynamics of instability in zeolitic materials.
623 Journal of Physics: Condensed Matter, 16, S3459-S3472.
624 Gregorkiewitz, M. (1984) Crystal-structure and Al/Si-ordering of a synthetic nepheline. Bulletin
625 De Mineralogie, 107, 499-507.
626 Hagaman, E.W., Jiao, J.A., Chen, B.H., Ma, Z., Yin, H.F., and Dai, S. (2010) Surface alumina

627 species on modified titanium dioxide: A solid-state ^{27}Al MAS and 3QMAS NMR
628 investigation of catalyst supports. Solid State Nuclear Magnetic Resonance, 37, 82-90.
629 Haines, J., Levelut, C., Isambert, A., Hebert, P., Kohara, S., Keen, D.A., Hammouda, T., and
630 Andrault, D. (2009) Topologically ordered amorphous silica obtained from the collapsed
631 siliceous zeolite, silicalite-1-F: A dtep toward "perfect" glasses. Journal of the American
632 Chemical Society, 131, 12333-12338.
633 Hay, R.L., and Sheppard, R.A. (2001) Occurrence of zeolites in sedimentary rocks: An overview.
634 In D.L. Bish, and D.W. Ming, Eds., Natural zeolites: Occurrence, properties, applications,
635 45, p. 217-234. Reviews in Mineralogy and Geochemistry, Mineralogical Society of
636 America, Chantilly, Virginia.
637 Henderson, C.M.B., and Taylor, D. (1979) Infrared-spectra of aluminogermanate-sodalite and
638 aluminate-sodalite and a re-examination of the relationship between T-O bond length, T-
639 O-T angle and the position of the main IR absorption-band for compounds with
640 framework structures. Spectrochimica Acta Part A: Molecular and Biomolecular
641 Spectroscopy, 35, 929-935.
642 Herrero, C.P., Sanz, J., and Serratosa, J.M. (1985) Si,Al distribution in micas; Analysis by high-
643 resolution ^{29}Si NMR spectroscopy. Journal of Physics C: Solid State Physics, 18, 13-22.
644 Hovis, G.L., Spearing, D.R., Stebbins, J.F., Roux, J., and Clare, A. (1992) X-ray powder
645 diffraction and ^{23}Na, ^{27}Al, and ^{29}Si MAS-NMR investigation of nepheline-kalsilite
646 crystalline solutions. American Mineralogist, 77, 19-29.
647 Kim, H.N., and Lee, S.K. (2013a) Atomic structure and dehydration mechanism of amorphous
648 silica: Insights from ^{29}Si and ^{1}H solid-state MAS NMR study of SiO_2 nanoparticles.
649 Geochimica et Cosmochimica Acta, 120, 39-64.
650 Kim, H.N., and Lee, S.K. (2013b) Effect of particle size on phase transitions in metastable
651 alumina nanoparticles: A view from high-resolution solid-state ^{27}Al NMR study.
652 American Mineralogist, 98, 1198-1210.

653 Kim, Y., Lee, S.K., and Kirkpatrick, R.J. (2010) Effects of intermediate range structure on the
654 ^{29}Si NMR chemical shifts of framework silicates: Results for analcime. American
655 Mineralogist, 95, 1694-1700.
656 Kirkpatrick, R.J. (1988) MAS NMR spectroscopy of minerals and glasses. In F.C. Hawthorne,
657 Ed., Spectroscopic methods in mineralogy and geology, 18, p. 341-403. Reviews in
658 Mineralogy and Geochemistry, Mineralogical Society of America, Chantilly, Virginia.
659 Kokotailo, G.T., and Fyfe, C.A. (1989) Zeolites; Unique materials for research and industry.
660 Journal of Physics and Chemistry of Solids, 50, 441-447.
661 Kosanovic, C., Subotic, B., and Ristic, A. (2004) Kinetic analysis of temperature-induced
662 transformation of zeolite 4A to low-carnegieite. Materials Chemistry and Physics, 86,
663 390-398.
664 Kosanovic, C., Subotic, B., Smit, I., Cizmek, A., Stubicar, M., and Tonejc, A. (1997) Study of
665 structural transformations in potassium-exchanged zeolite A induced by thermal and
666 mechanochemical treatments. Journal of Materials Science, 32, 73-78.
667 Lee, S.K. (2005) Microscopic origins of macroscopic properties of silicate melts and glasses at
668 ambient and high pressure: Implications for melt generation and dynamics. Geochimica
669 et Cosmochimica Acta, 69, 3695-3710.
670 Lee, S.K. (2010) Effect of pressure on structure of oxide glasses at high pressure: Insights from
671 solid-state NMR of quadrupolar nuclides. Solid State Nuclear Magnetic Resonance, 38,
672 45-57.
673 Lee, S.K., Kim, H.N., Lee, B.H., Kim, H.I., and Kim, E.J. (2010) Nature of chemical and
674 topological disorder in borogermanate glasses: Insights from ^{11}B and ^{17}O solid-state
675 NMR and quantum chemical calculations. The Journal of Physical Chemistry B, 114,
676 412-420.
677 Lee, S.K., and Stebbins, J.F. (1999) The degree of aluminum avoidance in aluminosilicate
678 glasses. American Mineralogist, 84, 937-945.

679 Lee, S.K., and Stebbins, J.F. (2000a) Al–O–Al and Si–O–Si sites in framework aluminosilicate
680 glasses with Si/Al=1: quantification of framework disorder. Journal of Non-Crystalline
681 Solids, 270, 260-264.
682 Lee, S.K., and Stebbins, J.F. (2000b) The structure of aluminosilicate glasses: High-resolution
683 ^{17}O and ^{27}Al MAS and 3QMAS. The Journal of Physical Chemistry B, 104, 4091-4100.
684 Lee, S.K., and Stebbins, J.F. (2009) Effects of the degree of polymerization on the structure of
685 sodium silicate and aluminosilicate glasses and melts: An ^{17}O NMR study. Geochimica et
686 Cosmochimica Acta, 73, 1109-1119.
687 Lee, S.K., and Weiss, C.A. (2008) Multiple oxygen sites in synthetic phyllosilicates with
688 expandable layers: ^{17}O solid-state NMR study. American Mineralogist, 93, 1066-1071.
689 Lee, S.K., Yi, Y.S., Cody, G.D., Mibe, K., Fei, Y.W., and Mysen, B.O. (2012) Effect of network
690 polymerization on the pressure-induced structural changes in sodium aluminosilicate
691 glasses and melts: ^{27}Al and ^{17}O solid-state NMR study. The Journal of Physical
692 Chemistry C, 116, 2183-2191.
693 Lippmaa, E., Magi, M., Samoson, A., Engelhardt, G., and Grimmer, A.R. (1980) Structural
694 studies of silicates by solid-state high-resolution ^{29}Si NMR. Journal of the American
695 Chemical Society, 102, 4889-4893.
696 Lippmaa, E., Magi, M., Samoson, A., Tarmak, M., and Engelhardt, G. (1981) Investigation of the
697 structure of zeolites by solid-state high-resolution ^{29}Si NMR-spectroscopy. Journal of the
698 American Chemical Society, 103, 4992-4996.
699 Lippmaa, E., Samoson, A., and Magi, M. (1986) High-resolution ^{27}Al NMR of aluminosilicates.
700 Journal of the American Chemical Society, 108, 1730-1735.
701 Loewenstein, W. (1954) The distribution of aluminum in the tetrahedra of silicates and
702 aluminates. American Mineralogist, 39, 92-96.
703 Lutz, W., Engelhardt, G., Fichtnerschmittler, H., Peuker, C., Loffler, E., and Siegel, H. (1985)
704 The influence of water steam on the direct phase transformation of zeolite NaA to

nepheline by thermal treatment. Crystal Research and Technology, 20, 1217-1223.

Madhu, P.K., Goldbourt, A., Frydman, L., and Vega, S. (1999) Sensitivity enhancement of the MQMAS NMR experiment by fast amplitude modulation of the pulses. Chemical Physics Letters, 307, 41-47.

Maekawa, H., Maekawa, T., Kawamura, K., and Yokokawa, T. (1991) The structural groups of alkali silicate-glasses determined from ^{29}Si MAS NMR. Journal of Non-Crystalline Solids, 127, 53-64.

Markovic, S., Dondur, V., and Dimitrijevic, R. (2003) FTIR spectroscopy of framework aluminosilicate structures: carnegieite and pure sodium nepheline. Journal of Molecular Structure, 654, 223-234.

Markovic, S., Dondur, V., Dimitrijevic, R., and Macura, S. (2006) Thermally induced rings formation in aluminosilicate structures. Journal of Thermal Analysis and Calorimetry, 84, 253-258.

Mimura, H., and Kanno, T. (1980) Processing of radioactive-waste solution with zeolites .1. Thermal-transformations of Na, Cs and Sr forms of zeolites. Science Reports of the Research Institutes Tohoku University Series a-Physics Chemistry and Metallurgy, 29, 102-111.

Mintova, S., and Bein, T. (2001) Nanosized zeolite films for vapor-sensing applications. Microporous and Mesoporous Materials, 50, 159-166.

Murdoch, J.B., Stebbins, J.F., Carmichael, I.S.E., and Pines, A. (1988) A silicon-29 nuclear magnetic resonance study of silicon-aluminum ordering in leucite and analcite. Physics and Chemistry of Minerals, 15, 370-382.

Neuhoff, P.S., Kroeker, S., Du, L.S., Fridriksson, T., and Stebbins, J.F. (2002a) Order/disorder in natrolite group zeolites: A ^{29}Si and ^{27}Al MAS NMR study. American Mineralogist, 87, 1307-1320.

Neuhoff, P.S., Shao, P., and Stebbins, J.F. (2002b) Effect of extraframework species on ^{17}O NMR

chemical shifts in zeolite A. Microporous and Mesoporous Materials, 55, 239-251.

Neuhoff, P.S., Stebbins, J.F., and Bird, D.K. (2003) Si-Al disorder and solid solutions in analcime, chabazite, and wairakite. American Mineralogist, 88, 410-423.

Neuville, D.R., Cormier, L., and Massiot, D. (2006) Al coordination and speciation in calcium aluminosilicate glasses: Effects of composition determined by ^{27}Al MQ-MAS NMR and Raman spectroscopy. Chemical Geology, 229, 173-185.

Newsam, J.M. (1987) Silicon-29 chemical shifts in sodalite materials. The Journal of Physical Chemistry, 91, 1259-1262.

Ohgushi, T., Ishimaru, K., and Komarneni, S. (2001) Nepheline and carnegieite ceramics from A-type zeolites by microwave heating. Journal of the American Ceramic Society, 84, 321-327.

Oliveira, A.C., Martins, L., and Cardoso, D. (2009) Basic catalytic properties of as-synthesized molecular sieves. Microporous and Mesoporous Materials, 120, 206-213.

Ori, S., Mazzucato, E., and Vezzalini, G. (2009) Dehydration dynamics of barrerite: An in situ synchrotron XRPD study. American Mineralogist, 94, 64-73.

Park, M.B., Vicente, A., Fernandez, C., and Hong, S.B. (2013) Solid-state NMR study of various mono- and divalent cation forms of the natural zeolite natrolite. Physical Chemistry Chemical Physics, 15, 7604-7612.

Peral, I., and Iniguez, J. (2006) Amorphization induced by pressure: Results for zeolites and general implications. Physical Review Letters, 97, 225502.

Phillips, B.L., Kirkpatrick, R.J., and Carpenter, M.A. (1992) Investigation of short-range Al,Si order in synthetic anorthite by ^{29}Si MAS NMR-spectroscopy. American Mineralogist, 77, 484-494.

Pilter, Z., Szabo, S., Hasznos-Nezdei, M., and Pallai-Varsanyi, E. (2000) X-ray diffraction study of the effect of microwave treatment of zeolite Na-A. Microporous and Mesoporous Materials, 40, 257-262.

Pingel, U.T., Amoureux, J.P., Anupold, T., Bauer, F., Ernst, H., Fernandez, C., Freude, D., and Samoson, A. (1998) High-field ^{17}O NMR studies of the SiOAl bond in solids. Chemical Physics Letters, 294, 345-350.

Ponyatovsky, E.G., and Barkalov, O.I. (1992) Pressure-induced amorphous phases. Materials Science Reports, 8, 147-191.

Radulovic, A., Dondur, V., Dimitrijevic, R., and Arandjelovic, D. (2010) Thermal transformation of Na-LTA zeolite into low-carnegieite: The influence of residual sodium and aluminium species. Thermochimica Acta, 511, 37-42.

Radulovic, A., Dondur, V., Vulic, P., Miladinovic, Z., Ciric-Marjanovic, G., and Dimitrijevic, R. (2013) Routes of synthesis of nepheline-type polymorphs: An influence of Na-LTA bulk composition on its thermal transformations. Journal of Physics and Chemistry of Solids, 74, 1212-1220.

Ramdas, S., and Klinowski, J. (1984) A simple correlation between isotropic ^{29}Si NMR chemical-shifts and T-O-T angles in zeolite frameworks. Nature, 308, 521-523.

Reed, T.B., and Breck, D.W. (1956) Crystalline zolites. 2.Crystal structure of synthetic zeolite, type A. Journal of the American Chemical Society, 78, 5972-5977.

Sabarinathan, V., Ramasamy, S., and Ganapathy, S. (2010) Perturbations to ^{27}Al electric field gradients in nanocrystalline a-Al_2O_3 studied by high-resolution solid-state NMR. The Journal of Physical Chemistry B, 114, 1775-1781.

Stebbins, J.F. (1988) NMR spectroscopy and dynamic processes in mineralogy and geochemistry. In F.C. Hawthorne, Ed., Spectroscopic methods in mineralogy and geology, 18, p. 405-429. Reviews in Mineralogy and Geochemistry, Mineralogical Society of America, Chantilly, Virginia.

Stebbins, J.F., Lee, S.K., and Oglesby, J.V. (1999a) Al-O-Al oxygen sites in crystalline aluminates and aluminosilicate glasses: High-resolution ^{17}O NMR results. American Mineralogist, 84, 983-986.

783 Stebbins, J.F., Murdoch, J.B., Carmichael, I.S.E., and Pines, A. (1986) Defects and short-range
784 order in nepheline group minerals: A ^{29}Si nuclear-magnetic-resonance study. Physics and
785 Chemistry of Minerals, 13, 371-381.
786 Stebbins, J.F., Oglesby, J.V., and Xu, Z. (1997) Disorder among network-modifier cations in
787 silicate glasses: New constraints from triple-quantum ^{17}O NMR. American Mineralogist,
788 82, 1116-1124.
789 Stebbins, J.F., Zhao, P.D., Lee, S.K., and Cheng, X. (1999b) Reactive Al-O-Al sites in a natural
790 zeolite: Triple-quantum oxygen-17 nuclear magnetic resonance. American Mineralogist,
791 84, 1680-1684.
792 Stoch, L., and Waclawska, I. (1994) Phase transformations in amorphous solids. High
793 Temperature Material Processes, 13, 181-201.
794 Stucky, G.D., Huo, Q., Firouzi, A., Chmelka, B.F., Schacht, S., Voigt-Martin, I.G., and Schüth, F.
795 (1997) Directed synthesis of organic/inorganic composite structures. In S.-K.I. Hakze
796 Chon, and U. Young Sun, Eds., Studies in Surface Science and Catalysis, 105, 3-28.
797 Elsevier, Amsterdam, Netherlands.
798 Thompson, J.G., Withers, R.L., Whittaker, A.K., Traill, R.M., and Fitz Gerald, J.D. (1993) A
799 reinvestigation of low-carnegieite by XRD, NMR and TEM. Journal of Solid State
800 Chemistry, 104, 59-73.
801 Utada, M. (2001) Zeolites in burial diagenesis and low-grade metamorphic rocks. In D.L. Bish,
802 and D.W. Ming, Eds., Natural zeolites: occurrence, properties, applications, 45, p. 277-
803 304. Reviews in Mineralogy and Geochemistry, Mineralogical Society of America,
804 Chantilly, Virginia.
805 Weller, M.T., Brenchley, M.E., Apperley, D.C., and Davies, N.A. (1994) Correlations between
806 ^{27}Al magic-angle spinning nucelar magnetic resonance spectra and the coordination
807 geometry of framework aluminates. Solid State Nuclear Magnetic Resonance, 3, 103-106.
808 Xu, Z., and Stebbins, J.F. (1998) Oxygen sites in the zeolite stilbite: a comparison of static, MAS,

809 VAS, DAS and triple quantum MAS NMR techniques. Solid State Nuclear Magnetic
810 Resonance, 11, 243-251.
811 Zhao, P., Neuhoff, P.S., and Stebbins, J.F. (2001) Comparison of FAM mixing to single-pulse
812 mixing in ^{17}O 3Q-and 5Q-MAS NMR of oxygen sites in zeolites. Chemical Physics
813 Letters, 344, 325-332.
814

FIGURE CAPTIONS

Figure 1. (a) Structure of Na-zeolite A showing secondary building units such as α-cage, β-cage (sodalite cage), and double four-membered rings (D4R). The crystallographically different oxygen sites are also described. The water molecules located inside the α- and β-cage are not shown (Baerlocher et al., 2007). (b) XRD patterns of Na-zeolite A and dehydrated phases with increasing annealing temperatures. Red (square), purple (circle), and blue (diamond) colors correspond to the peak positions and intensities of Na-zeolite A (JCPDS file no. 04-010-2001), low-carnegieite (Thompson et al., 1993), nepheline (JCPDS file no. 01-079-0992), respectively.

Figure 2. ^{29}Si MAS NMR spectra at 9.4 T of Na-zeolite A and dehydrated phases with increasing annealing temperatures up to 1173 K.

Figure 3. Simulation of ^{29}Si MAS NMR spectra at 9.4 T of Na-zeolite A and dehydrated phases with increasing annealing temperatures. Red, purple, blue, and black lines correspond to Q species in Na-zeolite A, low-carnegieite, nepheline, and amorphous phase, respectively.

Figure 4. ^{27}Al MAS NMR spectra at 9.4 T of Na-zeolite A and dehydrated phases with increasing annealing temperatures up to 1173 K.

Figure 5. ^{27}Al 3QMAS NMR spectra at 9.4 T of Na-zeolite A and dehydrated phases with increasing annealing temperatures up to 1173 K. Contour lines are drawn from 3 % to 98 % of relative intensity in increments of 5 %.

Figure 6. Isotropic projection of ^{27}Al 3QMAS NMR spectra of Na-zeolite A and dehydrated phases with increasing annealing temperatures up to 1173 K at 9.4 T.

Figure 7. Comparison of area-normalized ^{29}Si and ^{27}Al MAS NMR spectra of Na-zeolite A at 298 K and 873 K. The black and red lines refer to the NMR spectra at 298 K and 873 K, respectively.

Figure 8. ^{17}O 3QMAS NMR spectra of Na-zeolite A and dehydrated phases at 9.4 T with increasing annealing temperatures up to 1173 K. Contour lines are drawn from 8 % to 98 % of the relative intensity in increments of 5 %.

Figure 9. Isotropic projection of ^{17}O 3QMAS NMR spectra of Na-zeolite A and dehydrated phases with varying annealing temperatures at 9.4 T over the frequency range from (a) 0 to -60 ppm, and (b) -15 to -45 ppm.

Figure 10. ^{27}Al MAS NMR spectra of dehydrated Na-zeolite A at 873 K, prepared either in a glove box (black line) or an open atmosphere (red line).

Figure 11. (a) ^{17}O 3QMAS NMR spectra of dehydrated Na-zeolite A at 933 K immediately after annealing, and (b) seven months after annealing.

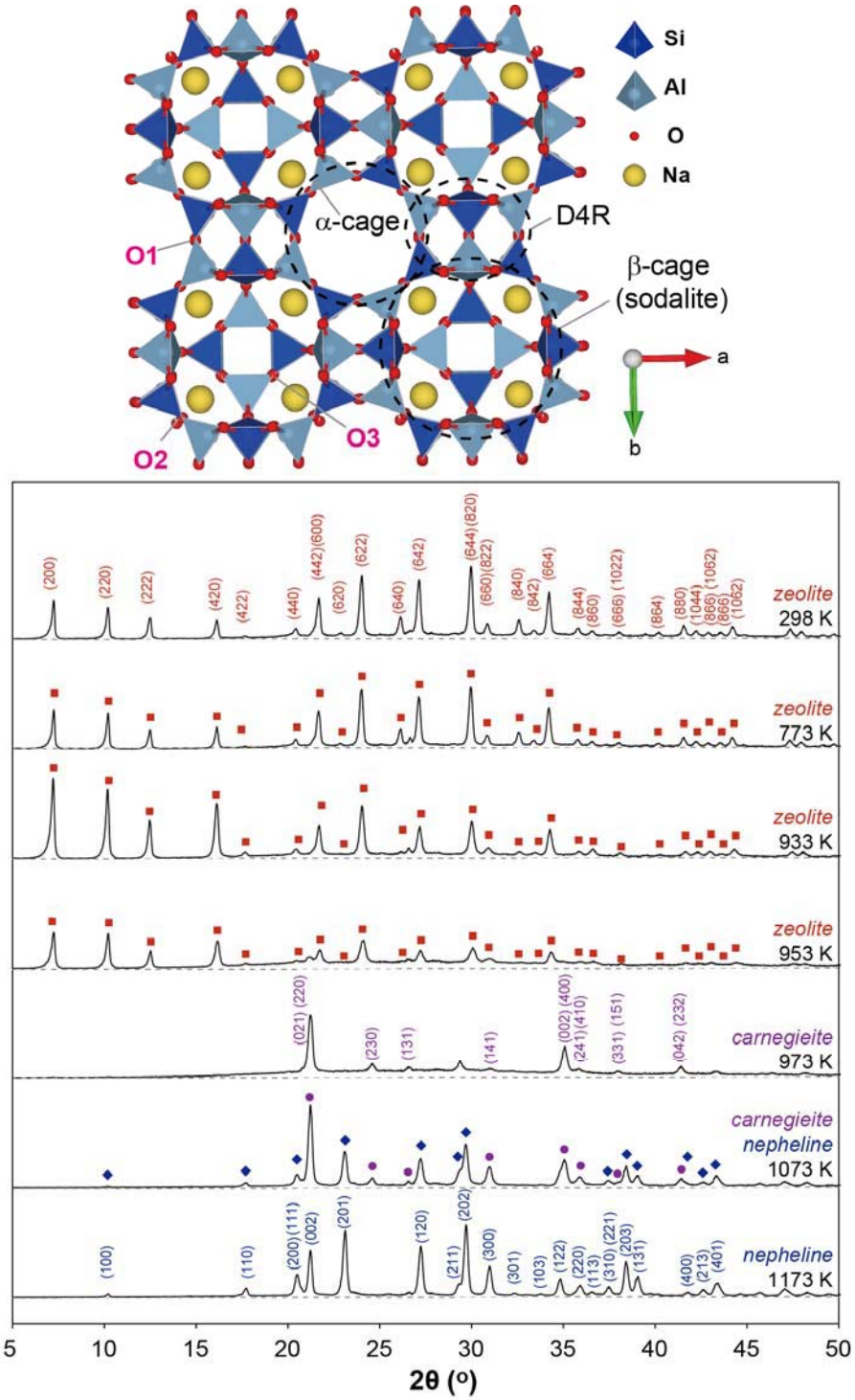

Figure 1

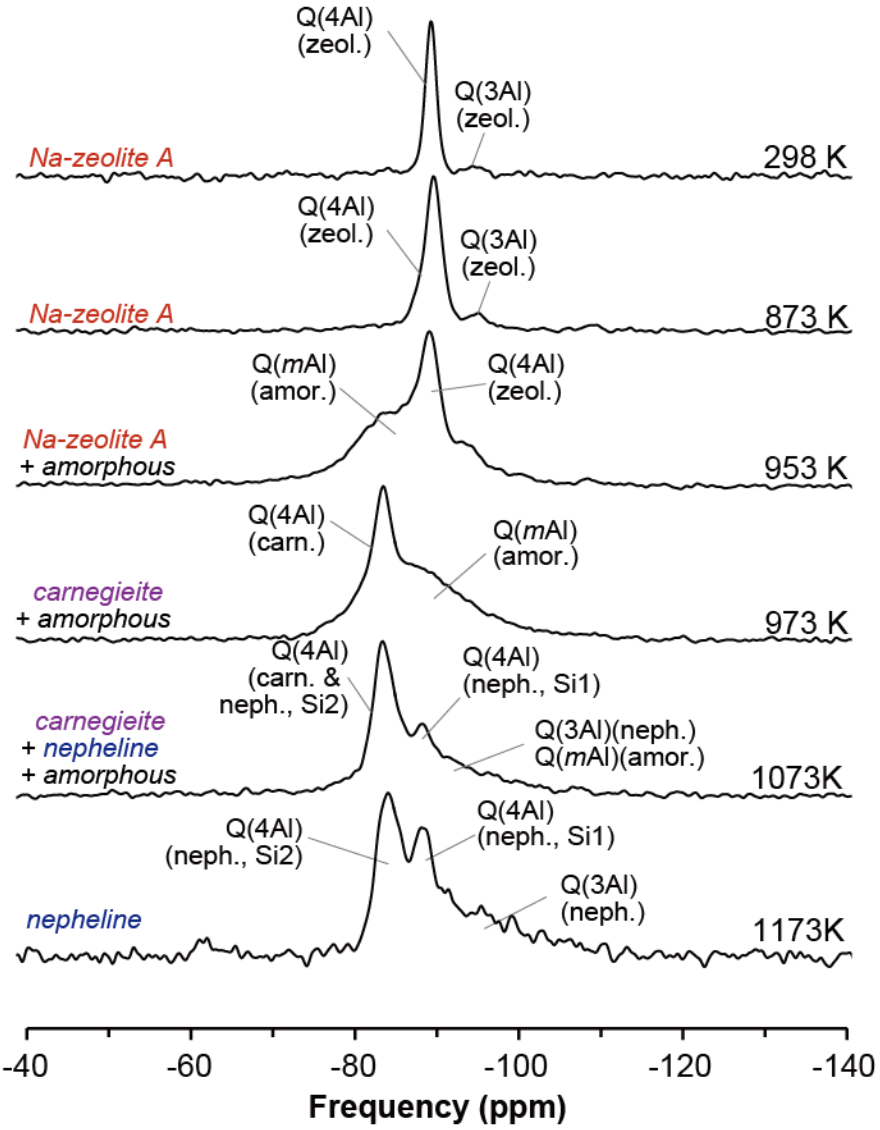

Figure 2

881

882

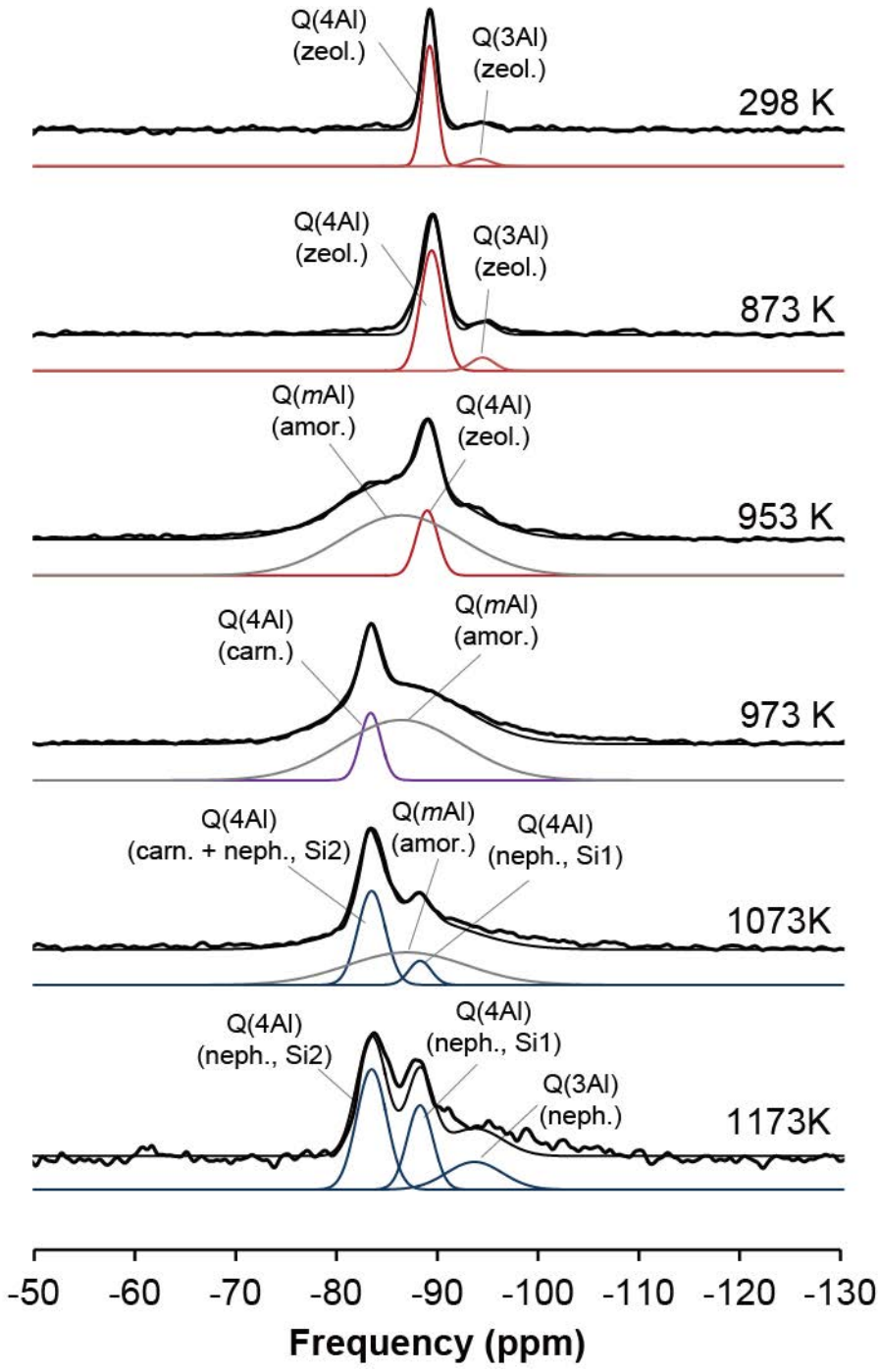

883

884

885 **Figure 3**

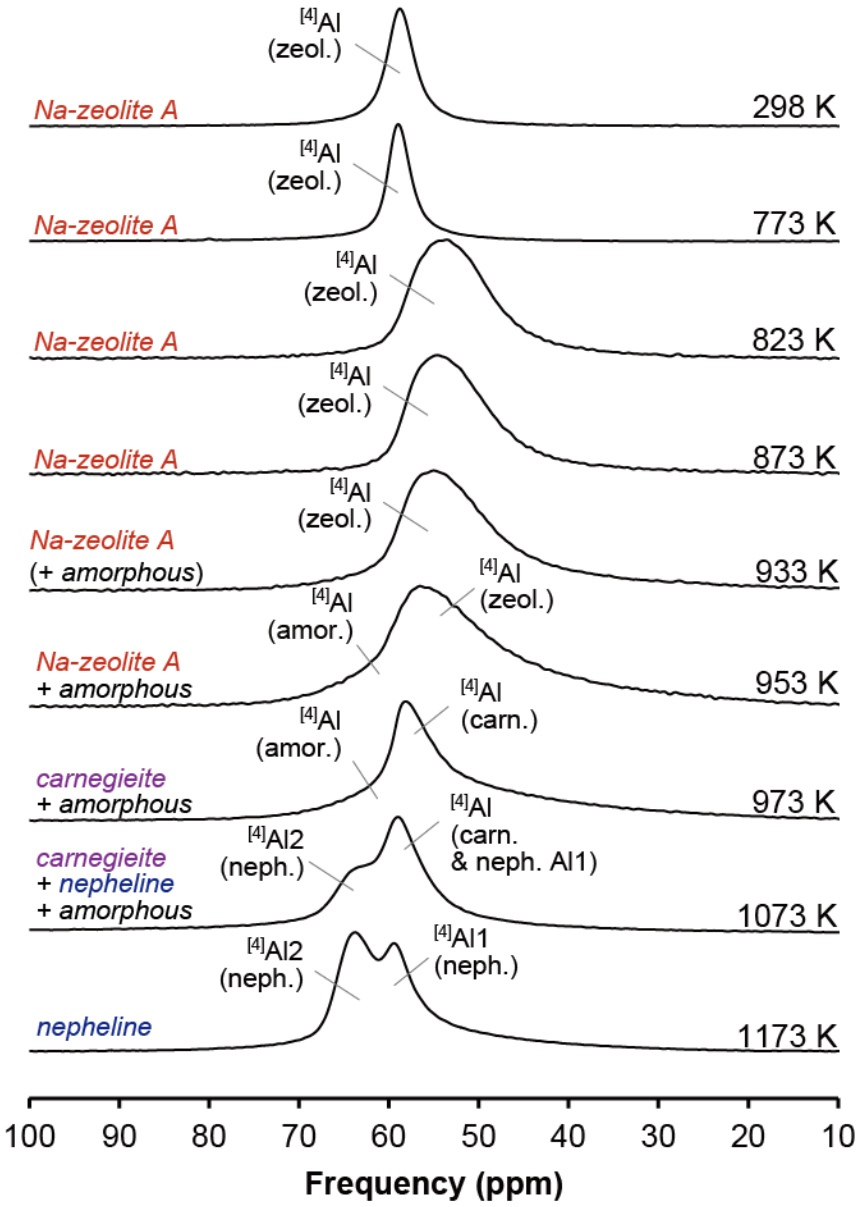

Figure 4

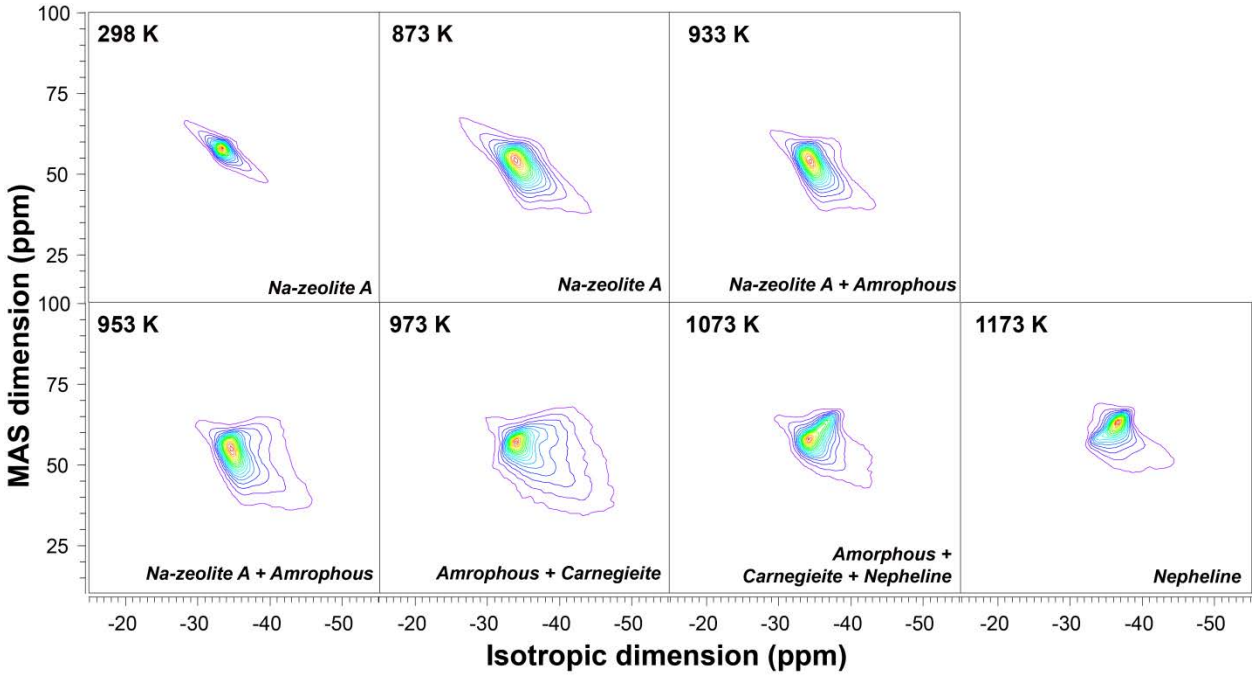

Figure 5

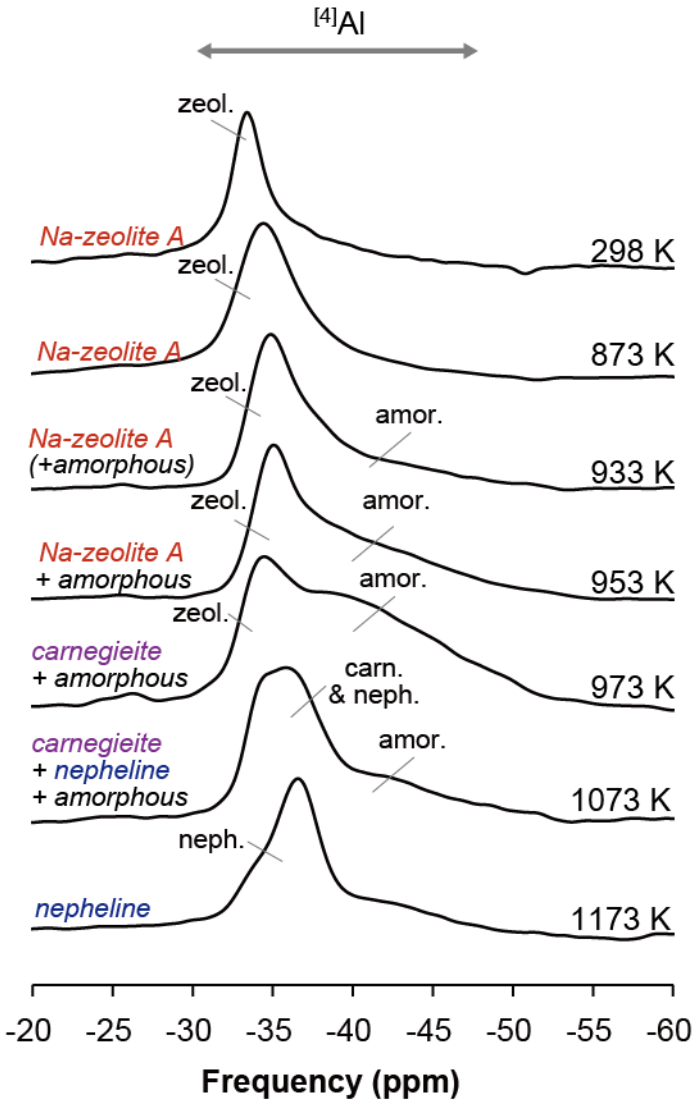

Figure 6

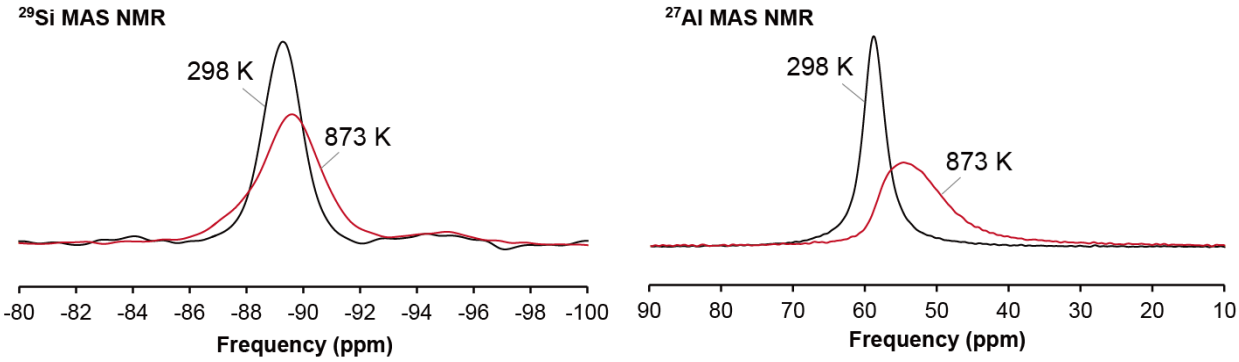

Figure 7

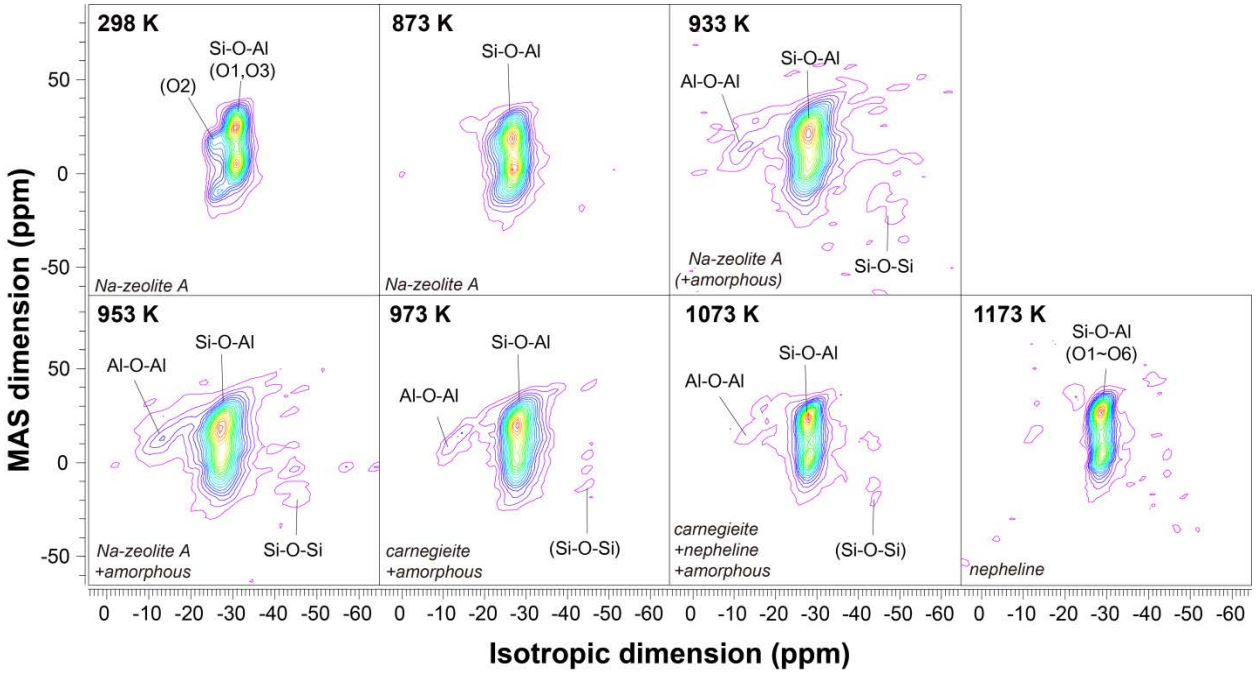

Figure 8

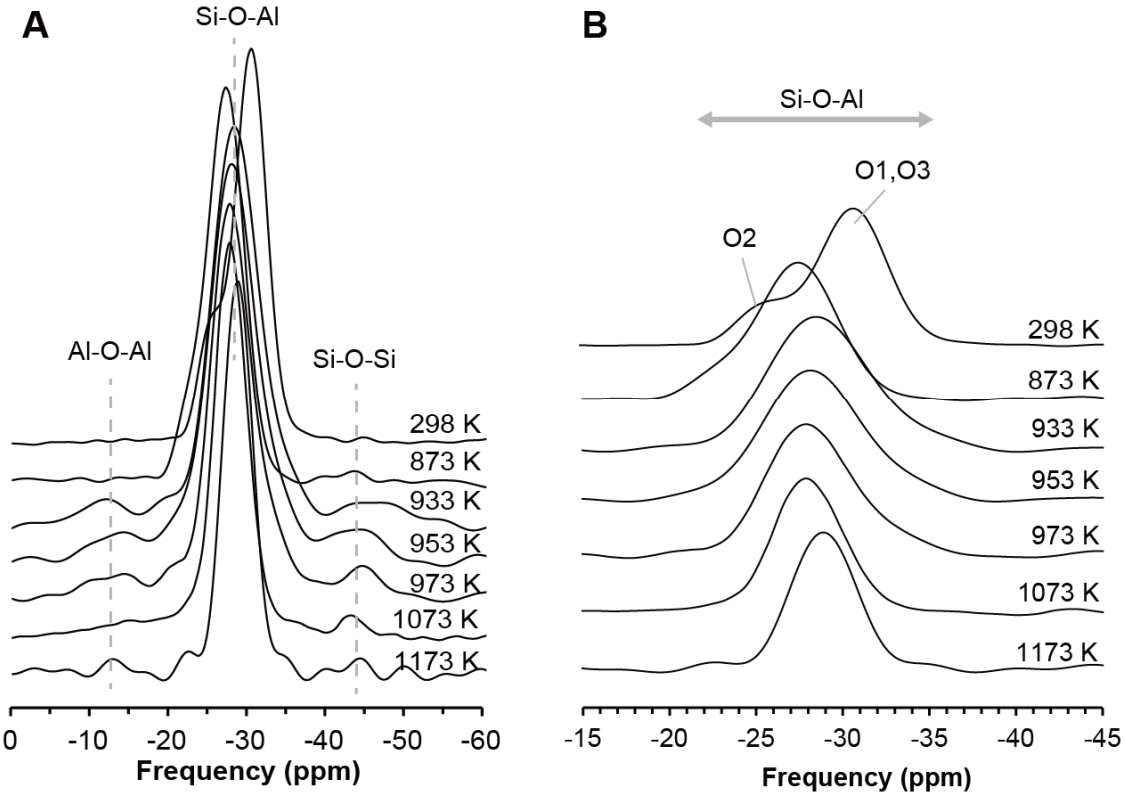

Figure 9

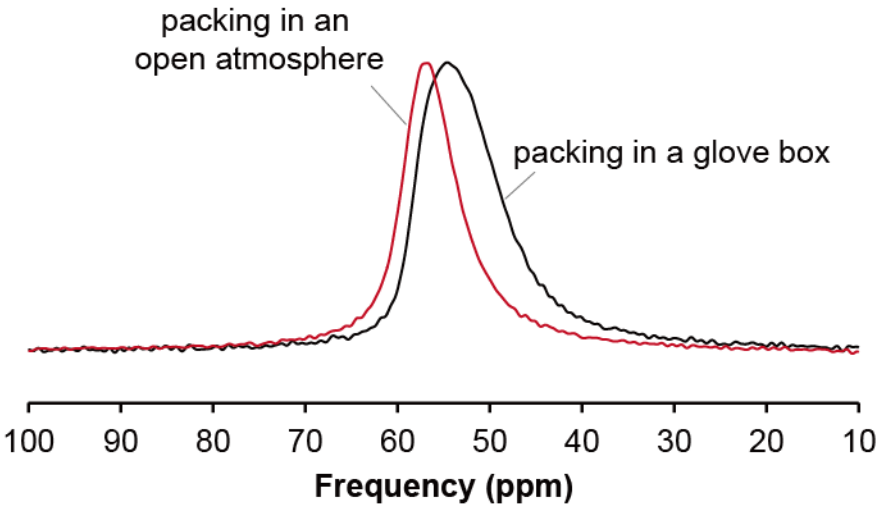

Figure 10

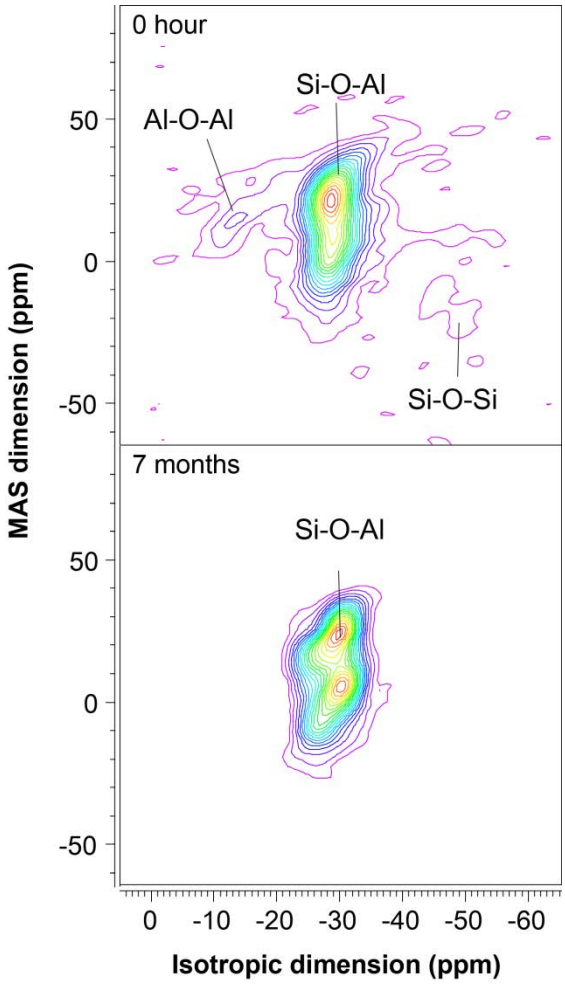

Figure 11